

## Incommensurate-modulated structure of nosean, a sodalite-group mineral

ISHMAEL HASSAN,\* PETER R. BUSECK

Departments of Geology and Chemistry, Arizona State University, Tempe, Arizona 85287, U.S.A.

### ABSTRACT

High-resolution transmission electron microscopy has provided evidence for ordering of  $[\text{Na}_4 \cdot \text{SO}_4]^{2+}$  and  $[\text{Na}_4 \cdot \text{H}_2\text{O}]^{4+}$  clusters in nosean, ideally  $\text{Na}_8[\text{Al}_6\text{Si}_6\text{O}_{24}]\text{SO}_4 \cdot \text{H}_2\text{O}$ . Reflections of type  $hhl$ ,  $l = 2n + 1$ , indicate that space group  $P\bar{4}3n$  is an average for nosean. Space group  $P23$ , a subgroup of  $P\bar{4}3n$ , applies to one type of domain that occurs in nosean and allows for a good model structure for nosean. These domains are based on ordering of the above clusters, and the domains are separated by antiphase domain boundaries. Domains that are based on positional modulations of the framework oxygen atoms also occur; some parts of the crystal show varying superstructure fringes that are absent in other parts. The complex satellite reflections arise from incommensurate modulations of the framework oxygen-atom positions in several directions and are prominent along  $(001)$ ,  $(110)$ ,  $(112)$ , and  $(41\bar{2})$ ; their periodicities differ with direction. The different sizes of the  $[\text{Na}_4 \cdot \text{SO}_4]^{2+}$  and  $[\text{Na}_4 \cdot \text{H}_2\text{O}]^{4+}$  clusters and their degree of ordering influence the positional modulations of the framework oxygen atoms. The cluster ordering, which is enhanced by the net charge differences between the clusters, accounts for the two well-defined framework oxygen-atom positions in nosean.

### INTRODUCTION

Many materials have the sodalite structure (Table 1). It is characterized by a framework of corner-linked  $\text{TO}_4$  tetrahedra ( $T = \text{Si}^{4+}$ ,  $\text{Al}^{3+}$ ,  $\text{Be}^{2+}$ ,  $\text{B}^{3+}$ ,  $\text{Ga}^{3+}$ , and  $\text{Ge}^{4+}$ ) and intervening large cages. Such cages are used as building blocks for many zeolites. The minerals of interest for this paper include the sulfate-rich sodalites (hauyne, lazurite, and, in particular, nosean). The ideal formula for nosean is  $\text{Na}_8[\text{Al}_6\text{Si}_6\text{O}_{24}]\text{SO}_4 \cdot \text{H}_2\text{O}$ .

The presence of complex satellite reflections from sulfate-rich sodalites is well established (Saalfeld, 1959, 1961; Schulz and Saalfeld, 1965; Taylor, 1967; Lohn and Schulz, 1968; Hassan et al., 1985). Saalfeld (1961) suggested that the superstructure in hauyne is related to interframework atomic order, and Schulz (1970) indicated that in the nosean structure all the atoms contribute to the superstructure reflections. Positional disorder has been reported for lazurite (Hassan et al., 1985). Saalfeld (1961) suggested that the nosean superstructure is commensurate, having a supercell six times that of the subcell, but Ito and Sadanaga (1966) interpreted the same superstructure in terms of multiple twinning of an orthorhombic cell. Taylor (1967) measured superstructure periodicities of nine specimens of sulfate-rich sodalites and found that their superstructures are incommensurate. The ratios of the published superstructure to subcell spacings range from 4.65 to 8.04. Details of satellite reflections from sulfate-rich sodalites differ for each mineral and differ among

specimens from different localities. In addition to different chemistries, the satellite reflections are related to the temperature of formation of the minerals and the ordering processes that are associated with decreasing temperature.

The origin of the complex satellite reflections in sodalite-group minerals is not known. In the first phase of this project, the structures of a number of sodalite-group minerals have been refined using single-crystal X-ray diffraction techniques (Table 1). One of the aims was to provide accurate structural data to form a basis for evaluating and proposing superstructure models. Although the structures were refined from measured intensities of sublattice reflections, the resulting structures include the averaged effects of positional and compositional modulations, and thus they include information on the superstructures. The data from these structures, therefore, form a necessary starting point for understanding the superstructures of sodalite-group minerals.

Although electron microscopy has not previously been done on nosean, such studies were performed on the related mineral hauyne. A multidimensional modulation of the structure was suggested to explain the satellite reflections (Morimoto, 1978). Tsuchiya and Takéuchi (1985) showed selected-area electron diffraction (SAED) patterns for  $[110]$  and  $[111]$  zones of a hauyne from Laacher See, Germany. They interpreted a dark-field image from the  $[111]$  zone as domains with dimensions of the order of 500 to 1500 Å. They concluded that hauyne consists of incoherent domains in six orientations, each having a superstructure modulated along one of the  $\langle 110 \rangle$  directions and fringe periodicities of about 50 Å. They proposed a

\* Present address: Department of Geology, University of New Mexico, Albuquerque, New Mexico 87131, U.S.A.

TABLE 1. Materials with sodalite-type structures

Phase	Chemical formula	Cage clusters	S§	Space group	Cell (Å) <i>a</i>	<i>R</i>	Reference
Sodalite	Na <sub>8</sub> [Al <sub>6</sub> Si <sub>6</sub> O <sub>24</sub> ]Cl <sub>2</sub>	100% [Na <sub>4</sub> ·Cl] <sup>3+</sup>	N	<i>P</i> 4̄3 <i>n</i>	8.882	0.017	Hassan and Grundy (1984a)
Hackmanite	Na <sub>8</sub> [Al <sub>6</sub> Si <sub>6</sub> O <sub>24</sub> ]Cl <sub>2</sub>	100% [Na <sub>4</sub> ·Cl] <sup>3+</sup>	N	<i>P</i> 4̄3 <i>n</i>	8.877	0.035	Peterson (1983)
Basic sodalite	Na <sub>8</sub> [Al <sub>6</sub> Si <sub>6</sub> O <sub>24</sub> ](OH) <sub>2</sub> ·2H <sub>2</sub> O	100% [Na <sub>4</sub> ·OH·H <sub>2</sub> O] <sup>3+</sup>	N	<i>P</i> 4̄3 <i>n</i>	8.890	0.028	Hassan and Grundy (1983a)
Nosean	Na <sub>8</sub> [Al <sub>6</sub> Si <sub>6</sub> O <sub>24</sub> ](SO <sub>4</sub> ) <sub>2</sub> ·H <sub>2</sub> O	50% [Na <sub>4</sub> ·SO <sub>4</sub> ] <sup>2+</sup> 50% [Na <sub>4</sub> ·H <sub>2</sub> O] <sup>4+</sup>	Y	<i>P</i> 4̄3 <i>n</i> *	9.084	0.057	Hassan and Grundy (1989a)
Hauyne	Na <sub>4.5</sub> Ca <sub>2</sub> K <sub>1</sub> [Al <sub>6</sub> Si <sub>6</sub> O <sub>24</sub> ](SO <sub>4</sub> ) <sub>1.5</sub> (OH) <sub>0.5</sub>	75% [Na <sub>3</sub> Ca·SO <sub>4</sub> ] <sup>3+</sup> 25% [K <sub>2</sub> Ca·OH] <sup>3+</sup>	N, Y	<i>P</i> 4̄3 <i>n</i> *	9.166	0.036	Hassan (1983)
Lazurite	Na <sub>6</sub> Ca <sub>2</sub> [Al <sub>6</sub> Si <sub>6</sub> O <sub>24</sub> ](SO <sub>4</sub> ) <sub>1.4</sub> S <sub>0.6</sub>	71% [Na <sub>3</sub> Ca·SO <sub>4</sub> ] <sup>3+</sup> 29% [Na <sub>3</sub> Ca·S] <sup>3+</sup>	Y	<i>P</i> 4̄3 <i>n</i> *	9.105	0.070	Hassan et al. (1985)
Helvite	Mn <sub>8</sub> [Be <sub>6</sub> Si <sub>6</sub> O <sub>24</sub> ]S <sub>2</sub>	100% [Mn <sub>4</sub> ·S] <sup>6+</sup>	N	<i>P</i> 4̄3 <i>n</i>	8.291	0.024	Hassan and Grundy (1985)
Danalite	Fe <sub>8</sub> [Be <sub>6</sub> Si <sub>6</sub> O <sub>24</sub> ]S <sub>2</sub>	100% [Fe <sub>4</sub> ·S] <sup>6+</sup>	N	<i>P</i> 4̄3 <i>n</i>	8.232	0.024	Hassan and Grundy (1985)
Genthelvite	Zn <sub>8</sub> [Be <sub>6</sub> Si <sub>6</sub> O <sub>24</sub> ]S <sub>2</sub>	100% [Zn <sub>4</sub> ·S] <sup>6+</sup>	N	<i>P</i> 4̄3 <i>n</i>	8.109	0.028	Hassan and Grundy (1985)
Bicchulite	Ca <sub>8</sub> [Al <sub>6</sub> Si <sub>4</sub> O <sub>24</sub> ](OH) <sub>8</sub>	100% [Ca <sub>4</sub> ·4OH] <sup>4+</sup>	N	<i>I</i> 43 <i>m</i>	8.825	0.012	Sahl (1980)
Synthetic	Ca <sub>8</sub> [Al <sub>12</sub> O <sub>24</sub> ](WO <sub>4</sub> ) <sub>2</sub>	100% [Ca <sub>4</sub> ·O] <sup>6+</sup>	N	<i>I</i> 43 <i>m</i>	8.86	0.069	Ponomarev et al. (1971)
Synthetic	Ca <sub>8</sub> [Al <sub>12</sub> O <sub>24</sub> ](WO <sub>4</sub> ) <sub>2</sub>	100% [Ca <sub>4</sub> ·WO <sub>4</sub> ] <sup>6+</sup>	Y	<i>A</i> ba2	26.151†	0.041	Depmeier (1984)
Synthetic	Zn <sub>8</sub> [B <sub>12</sub> O <sub>24</sub> ]O <sub>2</sub>	100% [Zn <sub>4</sub> ·O] <sup>6+</sup>	N	<i>I</i> 43 <i>m</i>	7.480	0.044	Smith-Verdier and Garcia-Blanco (1980)
Synthetic	Na <sub>8</sub> [Al <sub>6</sub> Ge <sub>6</sub> O <sub>24</sub> ](OH) <sub>2</sub>	100% [Na <sub>4</sub> ·OH] <sup>3+</sup>	N	<i>P</i> 4̄3 <i>n</i>	9.029	0.048	Belokoneva et al. (1982)
Synthetic	Na <sub>8</sub> [Ga <sub>6</sub> Si <sub>6</sub> O <sub>24</sub> ](OH) <sub>2</sub> ·6H <sub>2</sub> O	100% [Na <sub>4</sub> ·OH·3H <sub>2</sub> O] <sup>3+</sup>	N	<i>P</i> 4̄3 <i>n</i>	8.856	0.084	McCusker et al. (1986)
Tugtupite	Na <sub>8</sub> [Al <sub>2</sub> Be <sub>2</sub> Si <sub>6</sub> O <sub>24</sub> ]Cl <sub>2</sub>	100% [Na <sub>4</sub> ·Cl] <sup>3+</sup>	N	<i>I</i> 4	8.640‡	0.023	Hassan (1983); Danø (1966)

§ S = Satellite reflections: N = no, Y = yes.

\* Average space groups because these minerals may contain antiphase domain boundaries; the space group for each domain is *P*23.

† *b* = 13.075, *c* = 9.319.

‡ *c* = 8.873.

model based on a structure analysis of intensities obtained from domains that have a common orientation. Their model consists of intergrowths of a hauyne-like slab of five subcells and a nosean-like slab of three subcells. This model resembles that of *e*-plagioclase, which consists of slabs of anorthite-like and albite-like structures; the boundaries between the slabs are in antiphase relation. Consequently, the present study has analogies to and perhaps implications for the plagioclase feldspars.

This project entails the use of high-resolution transmission electron microscopy (HRTEM) to image the structures of sodalite materials showing complex satellite reflections. HRTEM imaging allows further modeling of the superstructures because both satellite and substructure reflections are used to form the image. In addition, in suitable cases, ordering can be determined, and if it is associated with antiphase domain boundaries (APBs), the latter can also be imaged. Moreover, electron diffraction allows distinction to be made between modulations resulting from atomic positions (= displacive modulations) vs. atomic substitution (= density modulations); sodalite-group and their polymorphic cancrinite-group minerals serve as ideal examples of these modulations. A preliminary report on the sulfate-rich sodalites and an aluminate, Ca<sub>8</sub>[Al<sub>12</sub>O<sub>24</sub>](CrO<sub>4</sub>)<sub>2</sub>, was given by Hassan and Buseck (1987).

Here we present HRTEM results on the ordering of [Na<sub>4</sub>·SO<sub>4</sub>]<sup>2+</sup> and [Na<sub>4</sub>·H<sub>2</sub>O]<sup>4+</sup> clusters in nosean; these clusters form domains that are separated by APBs. Domains based on positional modulations of the framework oxygen atoms also occur; some parts of the crystal show superstructure fringes that are absent in other parts. Our results suggest that the complex satellite reflections in nosean are

incommensurate and arise from the positional modulations of the framework atoms, particularly the two independent framework oxygen-atom positions. The positional modulations are related to the degree of ordering of clusters of different sizes, which is enhanced by the net charge differences of two valence units between the clusters.

#### STRUCTURES OF SODALITE-GROUP MINERALS

The cations in the TO<sub>4</sub> tetrahedra are fully ordered in the different sodalite frameworks, and the structures are characterized by sixfold rings of TO<sub>4</sub> tetrahedra parallel to {111} planes. These rings are stacked in a cubic ABCABC... sequence. The structures are further characterized by fourfold rings of TO<sub>4</sub> tetrahedra parallel to {100} planes. The linkage of the framework TO<sub>4</sub> tetrahedra results in a cubo-octahedral cage, called a β-cage in zeolite chemistry (Fig. 1a; also Fig. 1 of Hassan and Grundy, 1984a).

The net negative charge on the sodalite framework units can be neutralized by a large variety of interframework ions. The substitution is limited by the cage sizes and by the charge requirements of the framework units. The flexible sodalite cage adapts itself to different sizes of cage ions by cooperative rotation of the TO<sub>4</sub> tetrahedra (Beagley et al., 1982; Depmeier, 1984; Hassan and Grundy, 1984a). The two cages per unit cell in sodalite materials can order if the two types of clusters differ in either net charge or size. Such cluster ordering was reported for the scapolite-group minerals (Hassan and Buseck, 1988).

Sodalite materials that contain tetrahedral anion groups (e.g., SO<sub>4</sub><sup>2-</sup>, CrO<sub>4</sub><sup>2-</sup>, WO<sub>4</sub><sup>2-</sup>, etc.) exhibit complex satellite reflections. These materials include the sulfate-rich so-

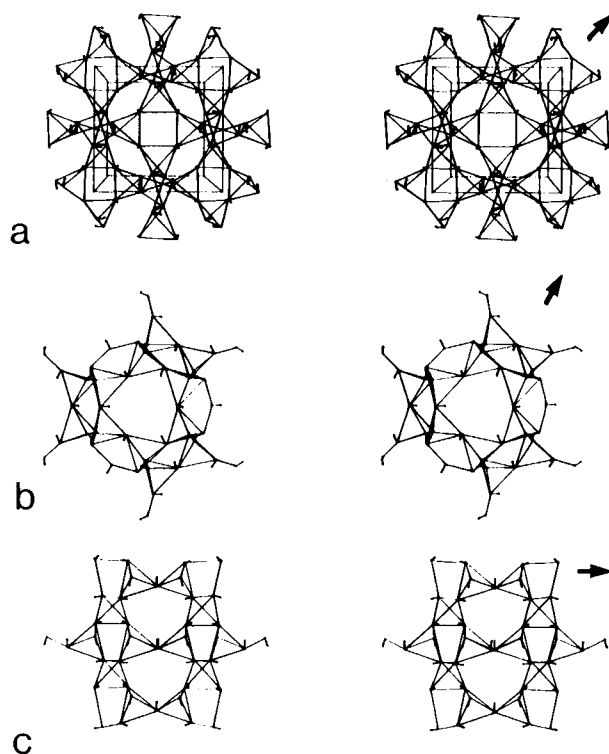


Fig. 1. Stereoscopic projections of approximately the upper half of the unit cell of nosean: (a) [001], (b) [111], and (c) [110] projections. The arrows point along a  $\langle 110 \rangle$  direction. The framework tetrahedra are based on the O1 oxygen-atom positions, and the short straight-line segments indicate displacements from O1 to O2 positions.

dalites and the aluminates,  $\text{Ca}_8[\text{Al}_{12}\text{O}_{24}](\text{SO}_4, \text{CrO}_4, \text{WO}_4)$  (Table 1). Sodalite materials that contain significant amounts of differently sized anions or cations (e.g.,  $\text{SO}_4^{2-}$  and  $\text{S}^{2-}$ ,  $\text{Li}^+$ , and  $\text{K}^+$ , or  $\text{K}^+$  and  $\text{Na}^+$ ) can also display complex satellite reflections. The occurrence of satellite reflections has been experimentally confirmed for anions that have different sizes (Table 1), but it has yet to be established for cations of different sizes.

The framework oxygen atoms of sodalite-group minerals in general are on a 24(i) site in space group  $P\bar{4}3n$ . However, in nosean and lazurite, they are disordered over two independent sets of 24(i) positions (O1 and O2). The interframework cations are generally on an 8(e) site on the body diagonals of the cubic structure, but in sulfate-rich sodalites, they are disordered over three independent sets of 8(e) positions that are close to each other. The 2(a) site at the centers of the cages contains the interframework anions (e.g.,  $\text{Cl}^-$  in sodalite). The  $\text{SO}_4^{2-}$  group can be in one or two orientations; one orientation is rotated  $90^\circ$  with respect to the other, and the interframework cations can force the S atom and thus the  $\text{SO}_4^{2-}$  group off the 2(a) site, as in hauyne (Hassan, 1983).

Figure 1 illustrates the relationship between the O1 and O2 framework oxygen-atom positions in the nosean

structure. Based on model calculations (Hassan and Grundy, 1984a, 1989a), the structure consisting of O1 oxygen atoms has a unit-cell edge that is  $0.26 \text{ \AA}$  shorter than one consisting of O2 oxygen atoms. This contraction can be seen in the four-membered rings (Fig. 1a) and in the six-membered rings (Figs. 1b, 1c). The contractions in nosean are three-dimensional; the maximum displacement components occur along directions such as  $\langle 001 \rangle$  (Figs. 1a, 1c) and  $\langle 110 \rangle$  (Fig. 1b) where strong satellite spots also occur in diffraction patterns, but there are displacement components in other directions as well. Alternatively, the displacements can be described as rotations, in opposite directions, of O1 and O2 tetrahedra from a more symmetrical, uncollapsed structure to these partially collapsed structures. Figure 2 of Hassan and Grundy (1984a) shows one set of these rotations in detail.

The satellite reflections in sulfate-rich sodalites are related to ordering on the O1 and O2 positions. This result follows partly from the observations that most sulfate-rich sodalites show similar disorder of the interframework ions. However, in some hauynes, the framework oxygen atoms are not positionally disordered because they occupy one set of 24(i) positions, but in nosean and lazurite they occupy two independent sets of 24(i) positions. Thus, satellite reflections are present in nosean and lazurite, but they are absent in some hauynes (Hassan, 1983; Hassan and Buseck 1989; Hassan and Grundy, 1989a).

#### ELECTRON MICROSCOPY

The nosean used in this study is from Laacher See, Germany (Royal Ontario Museum sample no. M5279) and was also used for structure refinement (Hassan and Grundy, 1983b, 1989a). The composition is close to ideal  $\text{Na}_8[\text{Al}_6\text{Si}_6\text{O}_{24}]\text{SO}_4 \cdot \text{H}_2\text{O}$ , and the cubic cell parameter,  $a_0$ , is  $9.084(2) \text{ \AA}$ .

Fragments of nosean were obtained by crushing in acetone using an agate mortar and pestle. The crystals in suspension were deposited on holey C support films, and HRTEM data were recorded from thin regions.

Preliminary electron microscopy (Figs. 7, 9, 10, 14) was performed using a JEOL 200CX microscope operated at 200 keV with a  $\text{LaB}_6$  filament and equipped with a  $\pm 12^\circ$  double-tilt, top-entry goniometer stage. The spherical aberration coefficient,  $C_s$ , of the objective lens was 1.2 mm. Various sizes of objective apertures were used in bright-field (BF), dark-field (DF), and multibeam HRTEM modes. A  $400\text{-}\mu\text{m}$  condenser aperture was used, and images were recorded at magnifications less than 270 000 in order to minimize the effects of beam damage. The sample was then re-examined in a JEOL 4000EX microscope (Figs. 8 and 11–13) operated at 400 keV, equipped with a  $\pm 15^\circ$  double-tilt, top-entry goniometer stage;  $C_s$  was 1.0 mm. HRTEM images were recorded at magnifications less than 250 000. Nosean did not damage as rapidly in the 4000EX as in the 200CX microscope because the former microscope was operated in the semi-automatic "minimum exposure" mode in order to minimize the electron-

beam irradiation. In this mode, the specimen is viewed on an attached TV screen (as in the 200cx microscope), but at minimum workable brightness. The moment the image is recorded, the electron beam converges automatically to produce images at a set exposure time of 2.8 s. After exposure, the electron beam is automatically deflected off the specimen, and the procedure is repeated for the next exposure.

### IMAGE SIMULATIONS

In our study of scapolite, we were able to distinguish contrast differences using HRTEM imaging, and the interpretations of ordering of  $[\text{Na}_4 \cdot \text{Cl}]^{3+}$  and  $[\text{NaCa}_3 \cdot \text{CO}_3]^{5+}$  clusters were confirmed by image simulations (Hassan and Buseck, 1988). These results suggest that clusters of  $[\text{Na}_4 \cdot \text{SO}_4]^{2+}$  and  $[\text{Na}_4 \cdot \text{H}_2\text{O}]^{4+}$  should also be distinguishable if they occur in nosean, so their ordering can be determined.

Simulations of high-resolution lattice images were obtained with the SHRLI set of programs (O'Keefe and Buseck, 1979; O'Keefe et al., 1978), which are based on the multislice method (Goodman and Moodie, 1974; Cowley and Moodie, 1957). Images were calculated for the [001], [110], and [111] zones over a range of defocus values and thicknesses. Calculations were performed using the electron optical parameters given above for the JEOL 4000EX microscope, together with a divergence angle of 0.8 milliradian, a depth of focus of 95 Å, and an objective aperture radius of  $0.6 \text{ \AA}^{-1}$  in reciprocal space.

Image simulations were made for an ordered model (ordered clusters) and a disordered model (disordered clusters). The disordered model is based on the average structure of nosean (Hassan and Grundy, 1983b, 1989a). For the ordered model, calculated lattice-fringe images are based on the ideal nosean model structure in space group  $P23$ , with the  $[\text{Na}_4 \cdot \text{SO}_4]^{2+}$  and  $[\text{Na}_4 \cdot \text{H}_2\text{O}]^{4+}$  clusters ordered around the center and corners of the cubic cell, respectively. In this model, one of the four possible positions for the oxygen atom of  $\text{H}_2\text{O}$  was arbitrarily chosen, and the Na atom positions were determined by an analysis similar to that presented for lazurite and nosean (Hassan et al., 1985; Hassan and Grundy, 1989a). This ordered structure was modeled in space group  $P1$  for the purpose of image calculations. All simulated images were printed on the same relative contrast scale.

Simulated images for the [001] and [110] zones are shown in Figure 2 for both models. The simulated images vary with defocus and thickness. The arrows mark rows that have different contrast intensities in the ordered model; these rows have identical contrast in the model where the clusters are disordered. The contrast differences are significant for the [001] image, but small differences occur for the [110] image. Therefore, clusters of  $[\text{Na}_4 \cdot \text{SO}_4]^{2+}$  and  $[\text{Na}_4 \cdot \text{H}_2\text{O}]^{4+}$  are distinguishable in computed nosean [001] images, so it should be possible to test the existence and pervasiveness of cluster order by HRTEM imaging.

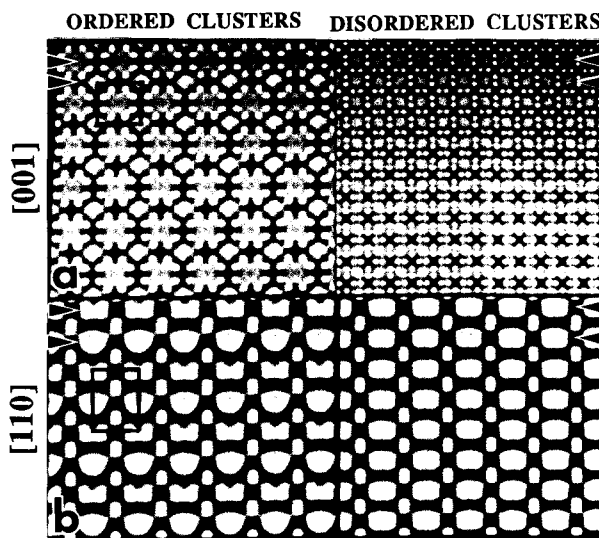


Fig. 2. Pairs of simulated images for (a) [001] and (b) [110] zones based on (1) ordering of  $[\text{Na}_4 \cdot \text{SO}_4]^{2+}$  and  $[\text{Na}_4 \cdot \text{H}_2\text{O}]^{4+}$  clusters around the centers and corners of the cell, respectively (left) and (2) disordering of clusters (right). The dark rows correspond to  $[\text{Na}_4 \cdot \text{SO}_4]^{2+}$  clusters and the light rows to  $[\text{Na}_4 \cdot \text{H}_2\text{O}]^{4+}$  clusters (a, left). The cell origins are at the top-left corners in each image. The defocus value for both pairs of images is  $-487 \text{ \AA}$  (optimum defocus), and the thicknesses are 91 and 96 Å for (a) and (b), respectively.

## ELECTRON DIFFRACTION

### SAED patterns of nosean

The nomenclature of Tsuchiya and Takéuchi (1985) is used to classify the observed reflections (Table 2). Figures 3 to 6 show SAED patterns for various zones in nosean. The nosean structure has a strong body-centered pseudosymmetry, so the main reflections can be classified into two groups: one group of strong reflections satisfies the body-centered missing rule and is called type  $p$  and the other group comprises weaker reflections and does not satisfy the rule: it is called type  $p'$ . Although space group  $P\bar{4}3n$ , which allows general reflections of the form  $hhl$ ,  $l = 2n$ , was assumed and used in the structure refinement, weak reflections of the form  $hhl$ ,  $l = 2n + 1$ , are present (e.g., 001 in Fig. 3).

The central region of the [001]-zone SAED pattern shows sharp main spots, diffuse streaking along  $\langle 110 \rangle^*$  directions, and no associated satellite reflections; around the edges are numerous satellite reflections with weak main spots (Fig. 3). Along the  $\mathbf{b}^*$  axis, satellite reflections, denoted " $u$ ," are displaced parallel to  $\mathbf{a}^*$ , and along the  $\mathbf{a}^*$  axis they are displaced parallel to  $\mathbf{b}^*$ . The magnitudes of these displacements and the intensities of the satellite reflections increase with increasing order of reflections, that is, toward the edges (Fig. 3). These characteristics indicate positional modulations (= displacive modulations; e.g., Smith, 1974, p. 127–137; Buseck and Cowley, 1983).

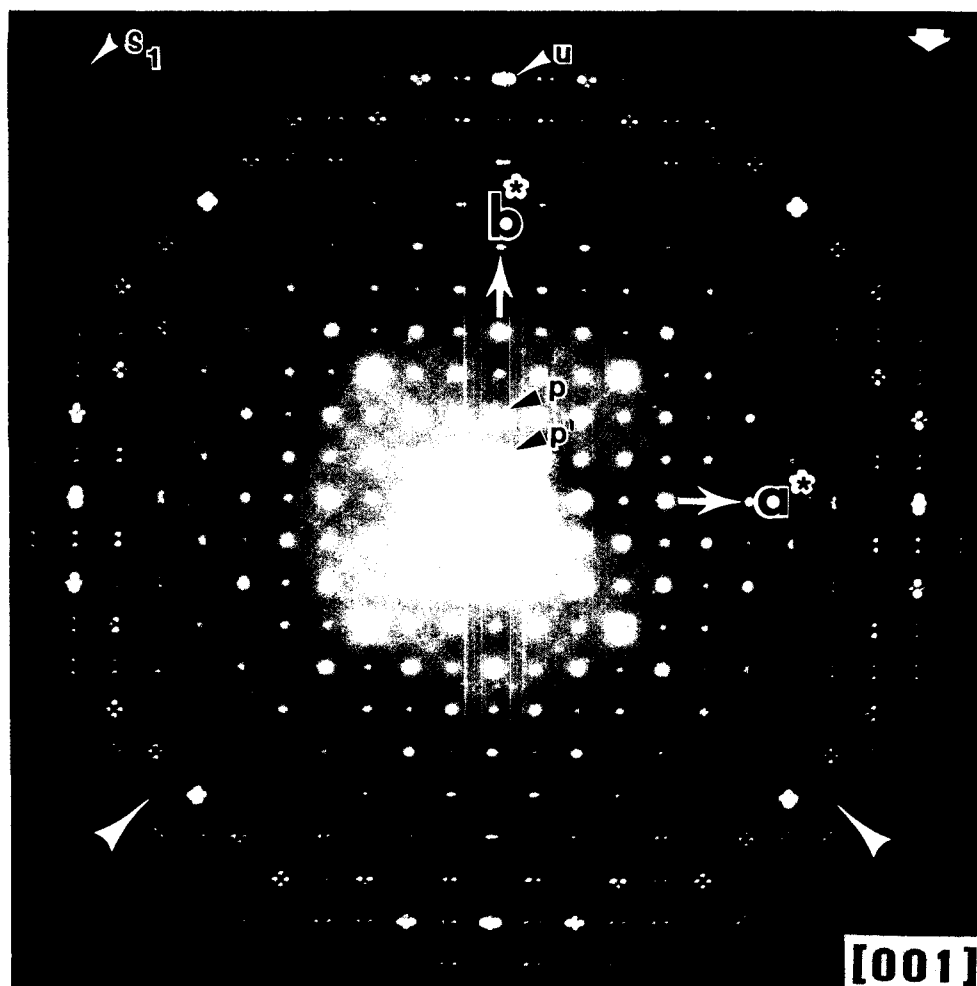


Fig. 3. [001]-zone SAED pattern of nosean.  $s_1$  and  $u$  satellite reflections occur around the edges. The arrow at the upper-right corner shows a group of  $s_1$  and  $u$  reflections. Alternating rows of weak  $p'$  reflections are best seen by viewing at a low angle along  $\langle 110 \rangle^*$  directions (arrows).

In the [110]-zone SAED pattern, a series of satellite reflections occur along a  $\langle 110 \rangle^*$  direction and may be visualized as a "splitting" of  $s_1$ ,  $s_2$ , and  $r$  reflections parallel to  $\langle 112 \rangle^*$  directions (Fig. 4; arrow 2 points out the split-

ting). A group of  $q$  satellite reflections has the appearance of an "X," with the subcell spot at the intersection. With increasing order of reflections along horizontal rows, the subcell spots in these X-like reflections lose intensity to the  $q$  satellite reflections; similar effects occur for  $u$  reflections (Fig. 3). The separation of pairs of  $q$  satellite reflections increases (i.e., the X becomes bigger) as the order of reflection increases. These features are indicative of positional modulations and occur along  $\langle 112 \rangle$ ,  $\langle 110 \rangle$ , and  $\langle 100 \rangle$  directions. The modulation along  $\langle 100 \rangle$  can be characterized as transverse, those along  $\langle 110 \rangle$  as longitudinal, and those along  $\langle 112 \rangle$  as a combination of both (see Fig. 5-3 of Smith, 1974). Of particular importance is the absence of satellite reflections along  $\langle 111 \rangle^*$  directions, indicating that the interframework atoms are not positionally ordered along such directions in nosean.

The central region of the [111]-zone SAED pattern contains strong substructure spots, and around each are two related groups of six-pointed stars of  $s_1$  and  $s_2$  satellite reflections (Fig. 5). Weak  $q$  satellite reflections occur along

TABLE 2. Classification of reflections in SAED patterns of nosean

Zone	Fig.	Reflections	
		Satellites $^{\S}$	Ordering $^{\dagger}$
[001]	3	$s_1, u$	$p'$
[110]	4	$s_1, s_2, q, u$	$r$
[111]	5	$s_1, s_2, q$	$r$
[123]	6	others $^{\ddagger}$	

$^{\S}$   $s_1$  and  $s_2$  are 1st- and 2nd-order reflections; they are parallel to the  $\langle 110 \rangle^*$  directions.  $u$  and  $q$  satellite reflections are parallel to  $\langle 001 \rangle^*$  and  $\langle 112 \rangle^*$  directions respectively.

$^{\dagger}$   $p'$  reflections are of the form  $hkl$ ,  $h + k + l = 2n + 1$  and  $p$  reflections are of the class  $hkl$ ,  $h + k + l = 2n$ .  $r$  reflections occur mid-way between main spots along  $\langle 110 \rangle^*$  directions.

$^{\ddagger}$  These include satellite reflections along  $\langle 412 \rangle^*$ ,  $\langle 331 \rangle^*$ , and  $\langle 032 \rangle^*$  directions.



Fig. 4. [110]-zone SAED pattern.  $s_1$ ,  $s_2$ ,  $q$ ,  $u$ , and  $r$  reflections are labeled. A group of  $s_1$ ,  $q$ , and  $u$  satellite spots are also shown (arrow 1). Note the divergence of pairs of satellite reflections (e.g., type  $u$ ) toward the edges.

$\langle 112 \rangle^*$  directions. The  $q$  satellite reflections are rotated by  $30^\circ$  with respect to the  $s_1$  reflections. Arrow 1 points out a group of  $s_1$  reflections with three visible spots—the main spot and two satellite spots. The other four satellite spots that complete the six-pointed star are faintly visible on the negative, so these seven spots are not  $q$  reflections. The difference in appearance between the central  $s_1$  spots and the  $s_1$  spots around the edges (Fig. 5) is probably related to the effect of curvature of the reflection sphere.

In general, the two-dimensional SAED patterns show one pair of satellites associated with  $h00$  reflections, two pairs for  $hk0$  reflections (Figs. 3, 4), and three pairs for  $hkl$  reflections (Fig. 5). There are weak “exceptions” ( $u$  and

$s_1$  arrows in Fig. 3). Pairs of satellites around main reflections have equal intensity. Strong satellite reflections occur along  $\langle 110 \rangle^*$ ,  $\langle 100 \rangle^*$ , and  $\langle 112 \rangle^*$  (Figs. 3, 4, 5), and so these are the principal modulation directions. These modulations can be correlated with O1-O2 displacements (Fig. 1). There are, however, alternative explanations for the satellites, as discussed below.

#### Effects from higher-order Laue zones (HOLZ)

Satellite reflections can arise from reciprocal lattice rods or spikes in HOLZ and can explain the divergence of pairs of satellite reflections with increasing order of reflection (see Hirsh et al., 1977, p. 323). However, use of stereo-

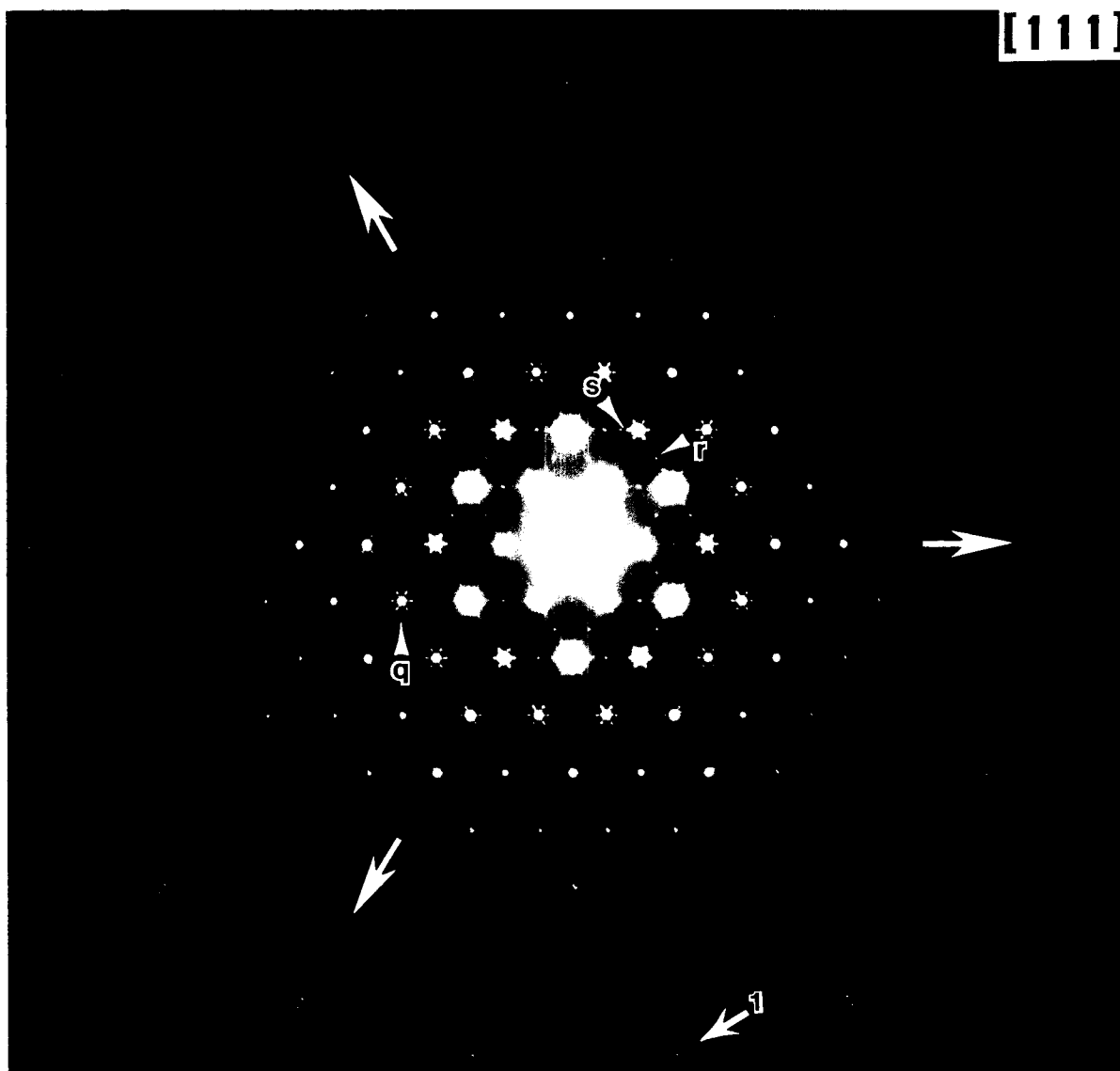


Fig. 5. [111]-zone SAED pattern. The large white arrows point along three  $\langle 110 \rangle^*$  directions.  $s_1$ ,  $s_2$  (labeled  $s$ ),  $q$ , and  $r$  reflections are labeled. The groups of  $s_1$  satellite reflections (arrow 1) occur around the edges of the figure.

graphic projections to examine this diffraction effect (e.g., Williams, 1984) indicates that the satellite reflections do not arise from HOLZ.

The [123]-zone SAED pattern shows satellite reflections in many directions (Fig. 6), and the corresponding images show superstructure fringes (not shown). Figures 3 and 4 show satellite reflections near the edges of the SAED patterns, whereas in Figures 5 and 6, the satellites occur in the central regions, supporting the interpretation that the satellites do not arise from reciprocal lattice spikes in HOLZ.

#### Diffraction from overlapping crystals

Another possible explanation for the satellite reflections in nosean is through double diffraction (= double

reflection), as suggested by Tsuchiya and Takéuchi (1985) for the  $q$  satellites. They explained double diffraction in terms of image sets. The effect is illustrated by Hirsh et al. (1977, p. 357–365) in a more conventional manner; we have adopted this method for the  $s_1$  reflections, but it applies equally well to the  $q$  reflections. In this approach, we are considering double diffraction from two parallel overlapping crystals (based on the experimental SAED patterns; e.g., Fig. 5) with slightly different lattice spacings, so the effect of parallel moiré fringes is considered.

Hirsh et al. (1977) illustrated that, for example, the  $s_1$  satellites (see Fig. 5) are equivalent to a Bragg reflection from a set of planes of interplanar spacing  $d_m = d_1 d_2 / |d_1 - d_2|$ , where  $d_1$  and  $d_2$  are the lattice spacings from the two overlapping crystals and  $d_m$  is the spacing of the moiré



Fig. 6. [123]-zone SAED pattern. Satellite reflections occur mainly along the  $\langle 412 \rangle^*$ ,  $\langle 331 \rangle^*$ , and  $\langle 032 \rangle^*$  directions (arrows), confirming that the nosean structure is modulated in many directions.

fringes. This result, in the case of cubic crystals, can also be written as  $d_m = a_1 a_2 / (a_1 - a_2)(h^2 + k^2 + l^2)^{1/2}$ , where  $a_1$  and  $a_2$  are the cubic cell parameters for the two overlapping lattices.

We now consider whether diffraction from overlapping crystals is applicable to nosean. The [111]-zone SAED pattern of nosean (Fig. 5) gives rise to  $d_1$  (main spots) and  $d_2$  ( $s_1$  satellite reflections) interplanar spacings of 6.42 Å ( $= d_{110}$  for nosean) and 5.63 Å, respectively. They correspond to  $a_1$  and  $a_2$  of 9.08 Å ( $= a_0$  for nosean) and 7.97 Å (assuming  $d_2$  is also from a 110 spot of a cubic crystal),

respectively. For these spacings, calculated moiré fringe spacings ( $d_m$ 's) of 65.2, 46.1, and 26.6 Å are expected for fringes parallel to  $\{001\}$ ,  $\{110\}$ , and  $\{112\}$  planes respectively, and they correspond respectively to  $u$ ,  $s_1$ , and  $q$  satellite reflections.

The nosean  $s_1$  satellite-reflection spacing more commonly is expressed as  $n \times d_{110}$  ( $= 6.5 \times 6.423 \text{ Å} = 41.75 \text{ Å}$ , based on X-ray precession photographs; Hassan and Grundy, 1989a). Because  $n$  is an irrational multiple of the basic structure, the nosean superstructure is incommensurate. The question arises whether the fringes cor-

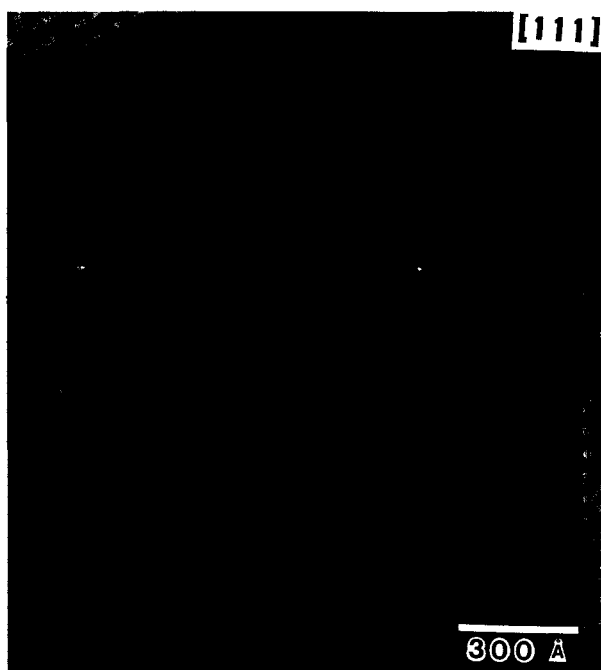


Fig. 7. [111] image of nosean. The three sets of intersecting superstructure fringes are parallel to  $\{110\}$  planes and intersect at  $60^\circ$ .

responding to the satellite reflections in nosean are moiré fringes that arise from overlapping crystals having slightly different lattices, or whether they are superstructure fringes arising from structural modulations.

The calculated cell parameters required to produce the observed nosean SAED patterns are 7.97 and 9.08 Å, if the satellites arise from two overlapping crystals. However, based on the model of Hassan and Grundy (1984a, 1989a), the calculated cell parameters are 9.20 Å ( $\text{SO}_4$ -bearing layer) and 8.94 Å ( $\text{H}_2\text{O}$ -bearing layer), values that are quite different from those obtained by double-diffraction calculations. Moreover, the average of the values obtained from the model is 9.07 Å, which is close to the measured cell value, 9.084 Å. These results indicate that the structures of sulfate-rich sodalites are not made up of slabs of different compositions, and so the slab model given above is not applicable to nosean (or any member of the sodalite group). Since the structure of nosean does not consist of slabs, it contrasts with the structure of *e*-plagioclase.

Equivalent pairs of  $s_1$  reflections that arise from overlapping slabs should have different intensities because they would arise from different combinations of spots and different thicknesses of slabs. However, pairs of  $s_1$  satellite reflections have equal intensity, as can be judged visually and as is confirmed by measurements made by Tsuchiya and Takéuchi (1985, p. 279). If the satellite reflections arise from different domains, then equality of intensity for pairs of satellite reflections is possible only if all domains have equal volumes in all crystals; a situation that

seems unlikely to occur in crushed grains. Moreover, the different types of satellite reflections in nosean are observed with X-rays (see Fig. 1 in Hassan and Grundy, 1989a), so they do not arise from double diffraction or HOLZ.

Having eliminated reciprocal lattice spikes from HOLZ and diffraction from overlapping slabs as possible explanations for the satellite reflections in nosean, we conclude that nosean consists of an incommensurate, modulated structure. To determine what periodic features give rise to the incommensurate modulations in nosean, we image the structure of nosean.

### TEM IMAGES OF NOSEAN

#### Superstructure lattice-fringes and type 1 domains

The [111] image contains three sets of superstructure fringes, each perpendicular to a  $\langle 110 \rangle$  direction and intersecting at  $60^\circ$ , having spacings of about 42 Å and corresponding to  $6.5 \times d_{110}$  (Fig. 7). Similar fringes occur in [111] images obtained in DF mode using a 110 reflection and its associated  $s_1$  satellite reflections. The fringes can be wavy, and "superstructure dislocations" occur in some images (e.g., Figs. 8 and 9). The fringes can be absent or in one, two, or three directions in different parts of [111] images; such regions can be considered as domains having ordering patterns that differ from each other, and they are called type 1 domains. The type 1 domains are related to the satellite reflections that arise from positional modulations of the framework oxygen atoms; the ordering of these atoms differs in parts of the crystal.

In places, the superstructure fringes show lateral offsets, thus indicating an out-of-phase boundary (Fig. 8a), which typically forms during ordering associated with decreasing temperature. In Figure 8b, which was taken after Figure 8a, the fringes are straight and continuous. The difference between these images indicates that the out-of-phase boundaries are mobile, and therefore they are presumably of low energy. The rearrangement of the superstructure fringes in the electron beam supports our model that the framework oxygen atoms are responsible for the modulations. These modulations are achieved through minor rotations of the framework tetrahedra (Fig. 1).

A set of  $s_1$  superstructure fringes occurs perpendicular to a  $\langle 110 \rangle$  direction (Fig. 9). They are several thousands of angstroms long, and they do not show significant lateral shifts, even though the fringes are wavy. Another image for this zone shows three sets of  $q$  and  $s_1$  superstructure fringes, but some of these fringes are absent in parts of the nosean crystal, thus indicating type 1 domains (Fig. 10; also Fig. 9). Other [110] images show complex mottling, with pronounced changes in contrast. The superstructure fringes are wavy and dislocations occur in the substructure, for example, the (110) fringes (not shown). In comparison, Figure 11 shows  $s_1$  superstructure fringes that are straight, and the image is not complex.

The thicker part of the crystal (Fig. 12a) contains  $s_1$

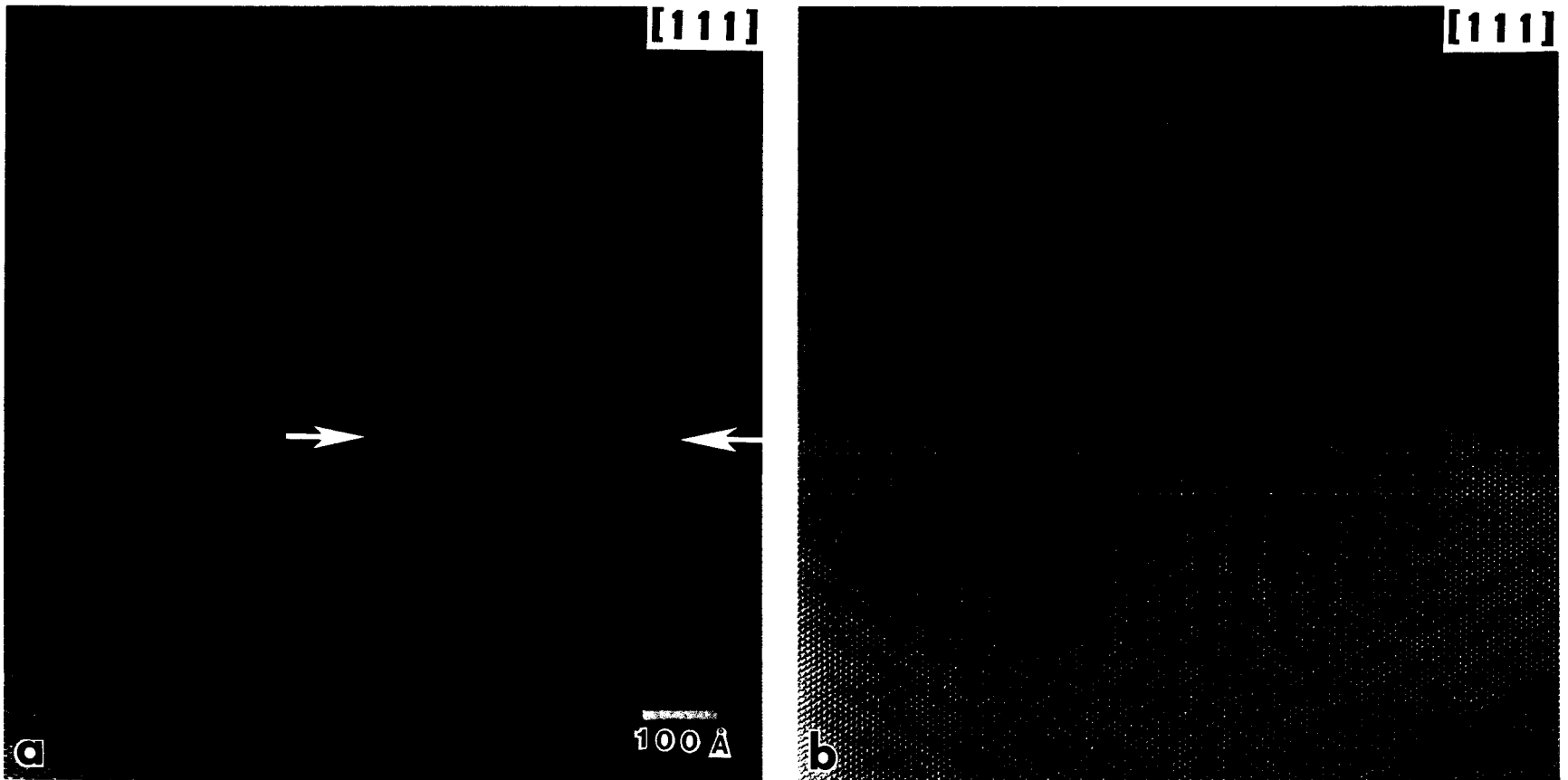
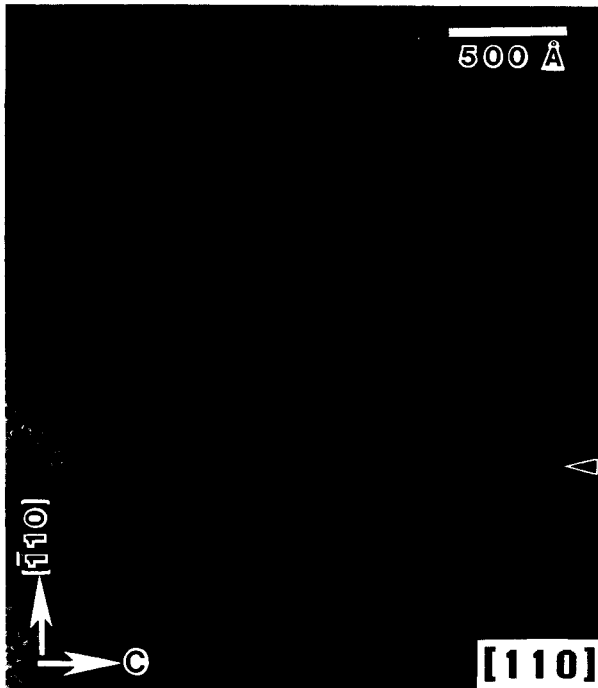


Fig. 8. Time-series  $[111]$  images from a nosean crystal. The superstructure fringes are shifted (best seen by sighting perpendicular to the arrows) in (a), but they are straight in (b), which was recorded a few seconds later.



superstructure fringes that are absent in the thinner part of the crystal. The optical diffractogram from the thinner part of the crystal (Fig. 12b; arrows) contains  $s_1$  satellite reflections, although in only one of the three possible  $\langle 110 \rangle^*$  directions. The channels that are parallel to the body diagonals of the cube are clearly visible (e.g., at the ends of the arrows in Fig. 12b). The variations in contrast of these channels indicate different chemistries. When these channels are ordered, they give rise to  $r$  reflections.

#### Cluster ordering and type 2 domains (APBs)

The simulated images (Fig. 2) indicate that ordered  $[\text{Na}_4 \cdot \text{SO}_4]^{2+}$  and  $[\text{Na}_4 \cdot \text{H}_2\text{O}]^{4+}$  clusters can be deduced by HRTEM imaging. Differences in contrast occur along (100) and (200), and (010) and (020) planes, respectively (arrows in Fig. 13). These differences arise from ordering of  $[\text{Na}_4 \cdot \text{SO}_4]^{2+}$  and  $[\text{Na}_4 \cdot \text{H}_2\text{O}]^{4+}$  clusters, as confirmed by image simulations based on this ordering model (central

←

Fig. 9.  $[110]$  image of nosean. Superstructure fringes are parallel to a  $\{110\}$  set of planes. The fringes are absent in some places. The arrow points out a superstructure dislocation.

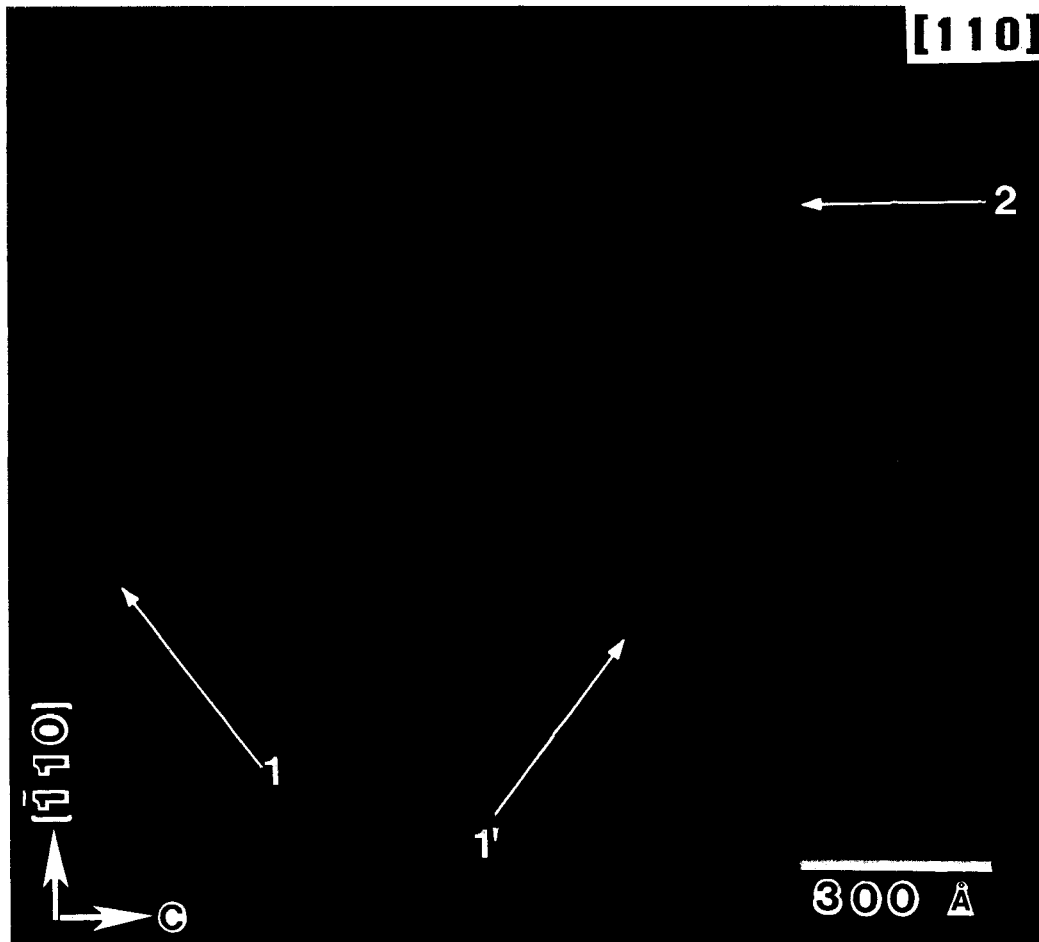


Fig. 10.  $[110]$  image showing three sets of superstructure fringes (parallel to the arrows). The related sets 1 and 1' (periodicity = 26.6 Å) are parallel to  $\{112\}$  planes, and set 2 is parallel to (110) planes.

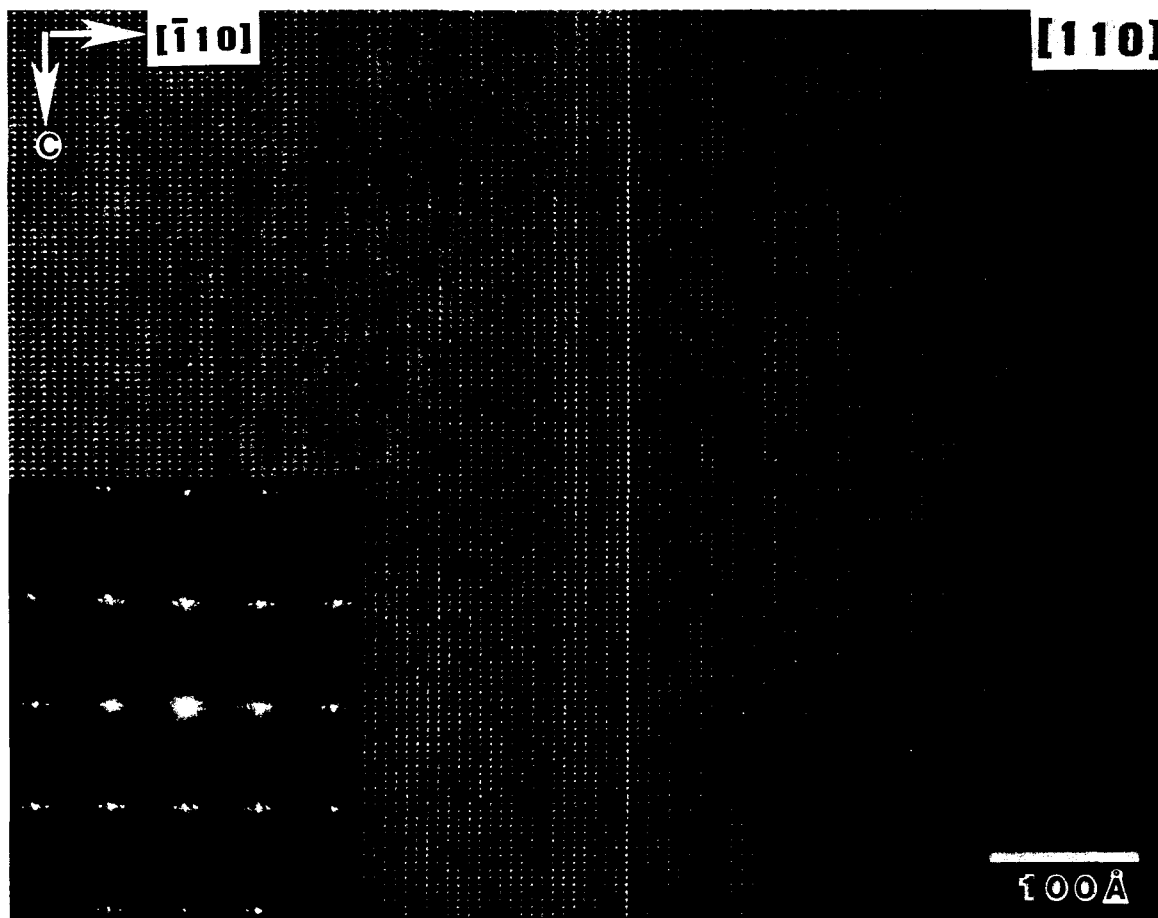


Fig. 11.  $[110]$  image of nosean. The optical diffractogram (insert) shows  $s_1$  satellite reflections, and the corresponding superstructure fringes appear parallel to  $c$  in the image.

insert in Fig. 13). Exposure of nosean to the electron beam causes disordering of the clusters, so care must be taken to observe such ordering (see Hassan and Buseck, 1989).

The observed ordering of  $[\text{Na}_4 \cdot \text{SO}_4]^{2+}$  and  $[\text{Na}_4 \cdot \text{H}_2\text{O}]^{4+}$  clusters can give rise to APBs in nosean, analogous to those in scapolite-group minerals. If the cavity at  $(0, 0, 0)$  is occupied by  $[\text{Na}_4 \cdot \text{SO}_4]^{2+}$  clusters, then the cavity at  $(\frac{1}{2}, \frac{1}{2}, \frac{1}{2})$  would be occupied by  $[\text{Na}_4 \cdot \text{H}_2\text{O}]^{4+}$  clusters; in the adjacent domain, the occupancy of the cavities is reversed. These domains are called type 2 domains, and they are separated by APBs. Figure 14 shows an APB across which the fringes are shifted by  $\frac{1}{2}a_0$ ; another  $[110]$  image shows an APB with a shift of  $\frac{1}{2}c_0$  (not shown). These APBs arise from cluster ordering, and the space group for each type 2 domain is  $P23$ .

#### DISCUSSION

The SAED patterns do not show satellite reflections along the  $\langle 111 \rangle^*$  directions, indicating that the interframework atoms do not order along these directions. The interframework cations and the oxygen atoms of the  $\text{SO}_4^{2-}$  group and  $\text{H}_2\text{O}$  are positioned on the body diagonals of

the nosean unit cell. However, the SAED patterns indicate that the nosean structure is modulated in several other directions, notably  $\langle 100 \rangle$ ,  $\langle 110 \rangle$ , and  $\langle 112 \rangle$ . The satellite reflections in nosean do not arise from substitutional ordering (= density modulations) or ordering of two physically different-size cages; such ordering cannot account for the divergence of pairs of satellites and increases in their intensities with increasing order of reflection. These characteristics are indicative of positional ordering (= displacive modulations) in nosean. In contrast, diffraction patterns for cancrinite-group minerals that are polymorphic with members of the sodalite-group minerals offer examples of substitutional ordering (Grundy and Hassan, 1982; Hassan and Grundy, 1984b, 1989b). For the cancrinite-group minerals, the density modulations of the interframework channel ions and their vacancies give rise to the satellite reflections.

A SAED pattern (e.g., Fig. 3) shows  $p'$  reflections (in particular,  $hhl$ ,  $l = 2n + 1$ ; e.g.,  $\{001\}$  reflections), and the corresponding image (Fig. 13) shows contrast suggestive of ordering of  $[\text{Na}_4 \cdot \text{SO}_4]^{2+}$  and  $[\text{Na}_4 \cdot \text{H}_2\text{O}]^{4+}$  clusters, implying that the contents of the cages centered at  $(0, 0,$

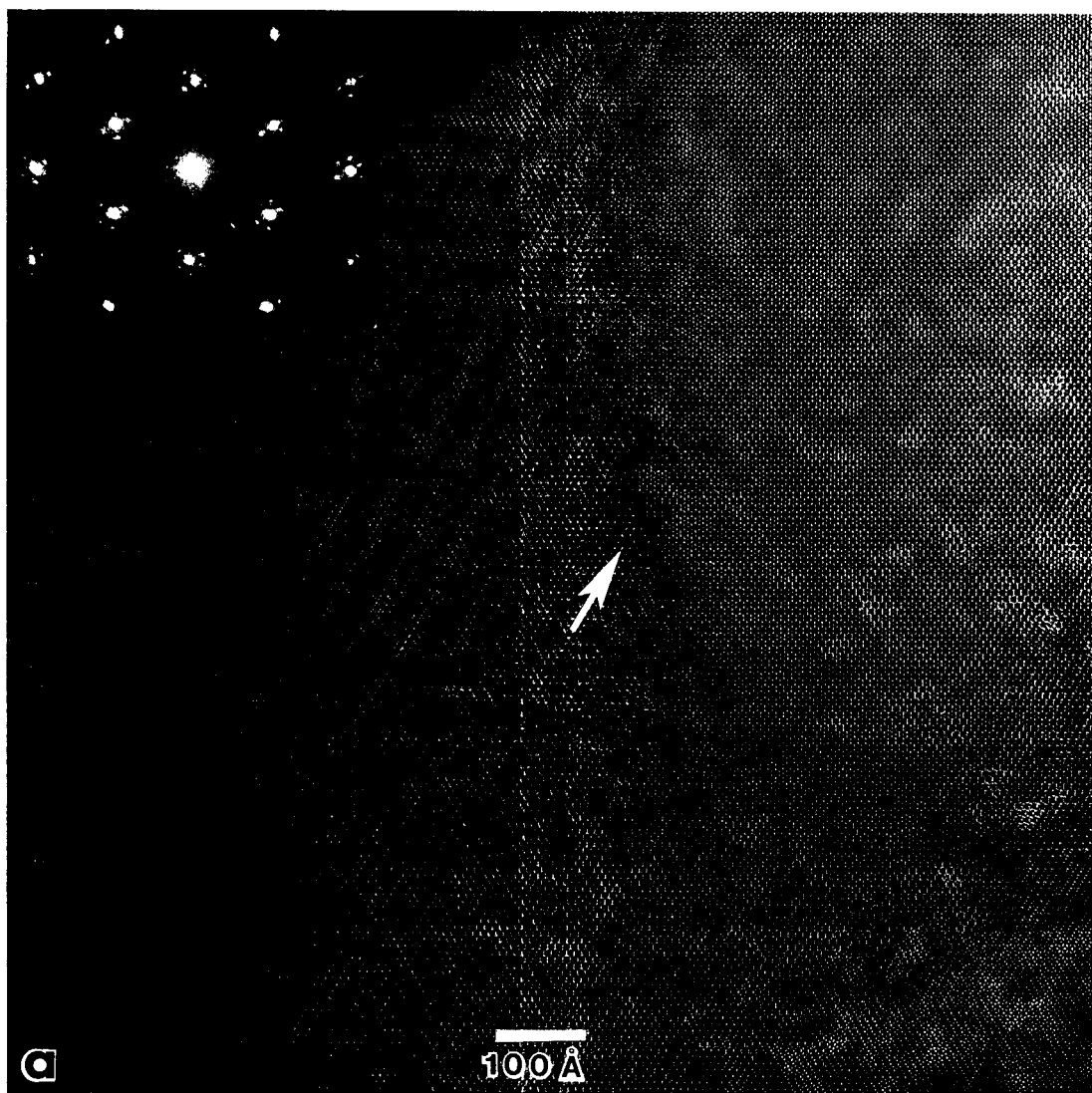


Fig. 12. [111] images of nosean. (a) Three sets of intersecting superstructure fringes, parallel to  $\{110\}$  planes, occur in the thicker part of the crystal (left), and the corresponding  $s_1$  satellite reflections are displayed in the optical diffractogram. A shift in fringe position, arising from thickness variations, is indicated (arrow). (b) Magnified image of the thinner part of the crystal (upper-

right of Fig. 14a). The contrast of the channels along [111] (arrows) differs from the others. The inserts give the simulated image (thickness = 131 Å; defocus = -400 Å), optical diffractogram, and structure projection. In the structure projection, the large open circles indicate the positions of the clusters and channel positions along [111].

0) and  $(\frac{1}{2}, \frac{1}{2}, \frac{1}{2})$  are not equivalent. Nosean contains type 2 domains that are separated by APBs that arise from cluster ordering, and so the average structure is best described in space group  $P\bar{4}3n$ . However, the  $p'$  reflections indicate that space group  $P23$ , a subgroup of  $P\bar{4}3n$ , is most appropriate for the individual domains. A model structure for nosean in space group  $P23$  is given by Hassan and Grundy (1989a).

The structures of nosean and lazurite are similar, and they also exhibit similar SAED patterns, so the results for nosean may be applicable to lazurite. The framework oxygen atoms in nosean and lazurite are positionally dis-

ordered over two independent sets of 24(i) positions in space group  $P\bar{4}3n$ , but this 24(i) site degenerates to two independent sets of 12-fold sites in space group  $P23$ . These 12-fold positions permit reasonable nosean and lazurite structures. The 8(e) and 2(a) sites in  $P\bar{4}3n$  give rise to 4- and 1-fold sites, respectively, in  $P23$ , so they allow for cluster ordering.

The TEM images of nosean show that the structure is modulated in several directions in different parts of the crystal, and some parts are unmodulated. In the different parts of the crystal, the framework oxygen atoms are positionally ordered in different ways on the O1 and O2

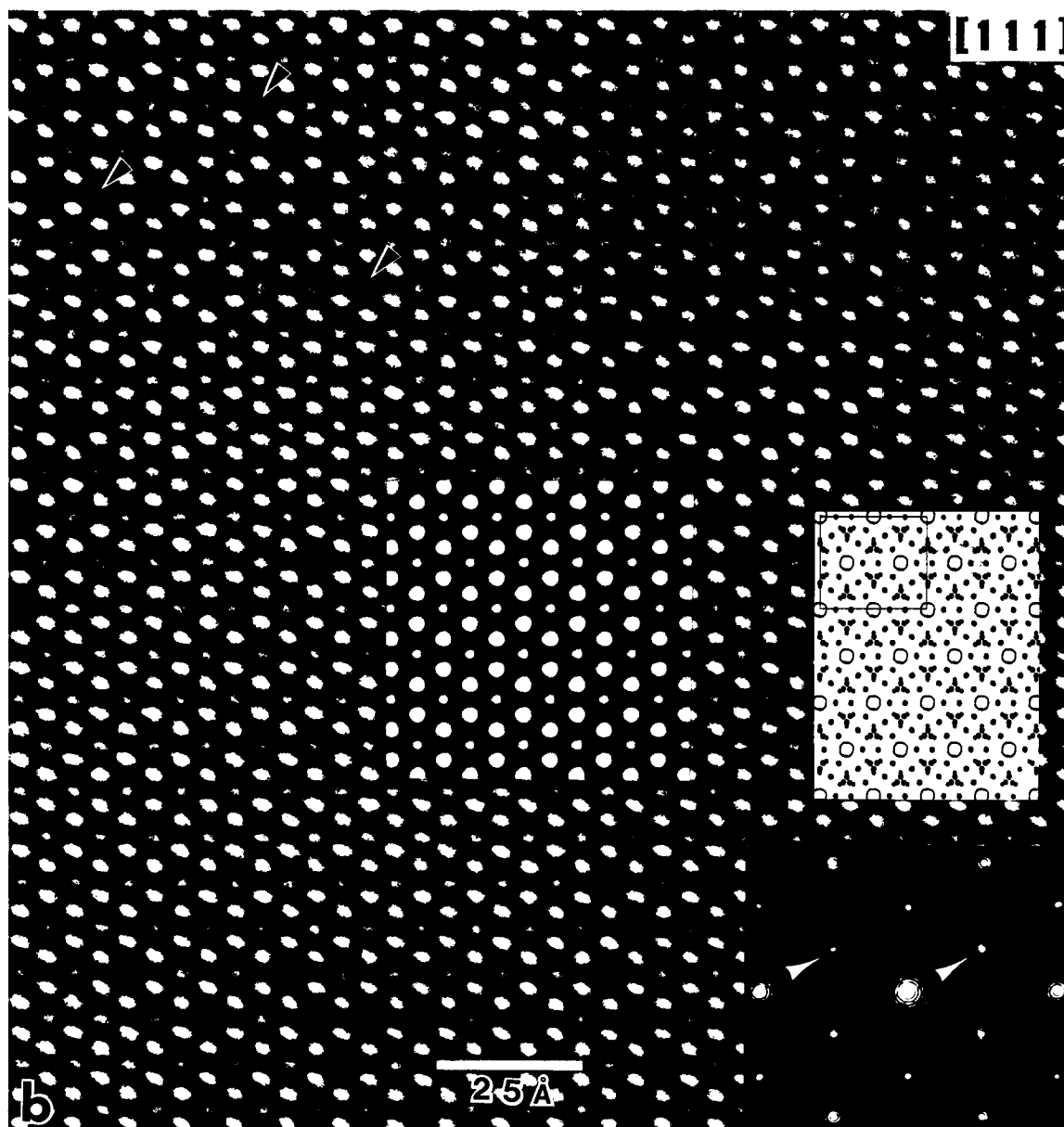


Fig. 12.—Continued.

positions (type 1 domains). The ordered ideal nosean  $P23$  domains correspond to unmodulated parts of the crystal that also contain cluster ordering (type 2 domains) and may be compared to a low-temperature form, whereas the type 1 domains can be considered analogous to one that is in a transitional state.

Our results provide the following scenario for the formation and transitions in nosean. At high temperature, clusters of  $[\text{Na}_4 \cdot \text{SO}_4]^{2+}$  and  $[\text{Na}_4 \cdot \text{H}_2\text{O}]^{2+}$  are randomly distributed, and the structure is consistent with space group  $P43n$ . On cooling, an ordering process is initiated and driven by differing spatial and charge requirements

between the clusters. During this intermediate stage, the clusters are partially ordered, and this causes the framework oxygen atoms to be positionally modulated and give rise to the satellite reflections of type 1 domains. In the final low-temperature stage, the clusters are fully ordered, and the structure conforms to space group  $P23$ , a subgroup of  $P43n$ ; no satellite reflections occur, so superstructure fringes are absent. Nosean  $P23$  domains could nucleate in different parts of the crystal, with the aluminosilicate framework remaining intact. Where the different parts of the crystal meet, APBs are formed.

The occurrence of satellite reflections and their mod-

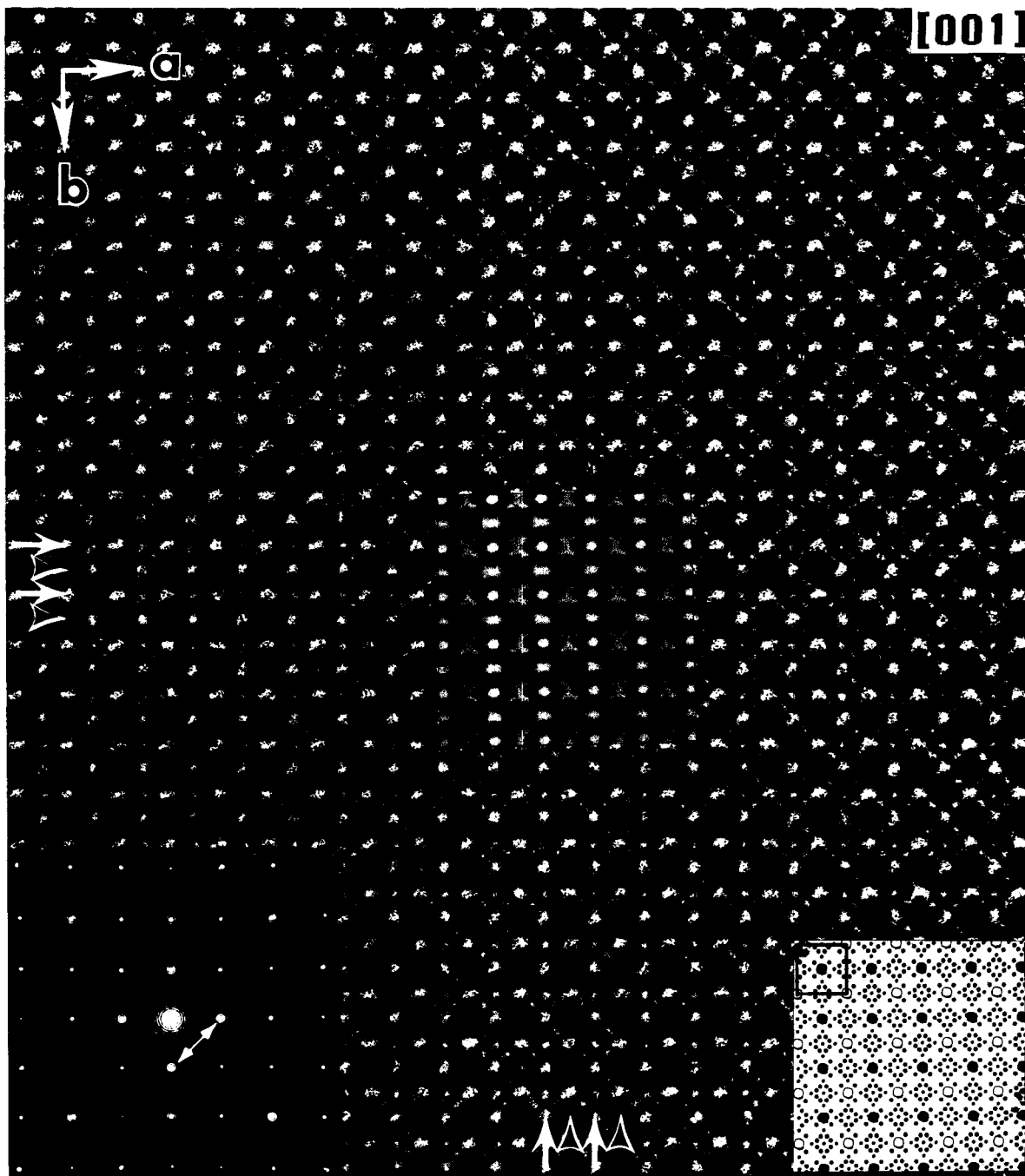


Fig. 13. [001] image of nosean. The optical diffractogram (insert) shows 010 and 100 ordering reflections (arrows). A unit cell is outlined in the structure projection ( $a_0 = 9.084 \text{ \AA}$ ). Ordering of  $[\text{Na}_4 \cdot \text{SO}_4]^{2+}$  and  $[\text{Na}_4 \cdot \text{H}_2\text{O}]^{++}$  clusters at the corners and center of the cubic cell is shown by black and white arrows that point out rows with different contrast. This ordering is also indicated in the structure projection by large open and filled circles and is confirmed by the inserted simulated image (thickness =  $182 \text{ \AA}$ ; defocus =  $-500 \text{ \AA}$ ).

ulation directions can be explained directly in terms of the crystal structure (Fig. 1). The displacement vectors between the O1 and O2 framework oxygen-atom positions have components in many directions, but their maxi-

mum displacement components occur in the same directions as the satellite reflections, namely,  $\langle 001 \rangle$ ,  $\langle 110 \rangle$ , and  $\langle 112 \rangle$ . The satellite reflections are, therefore, correlated with the framework oxygen-atom displacements.

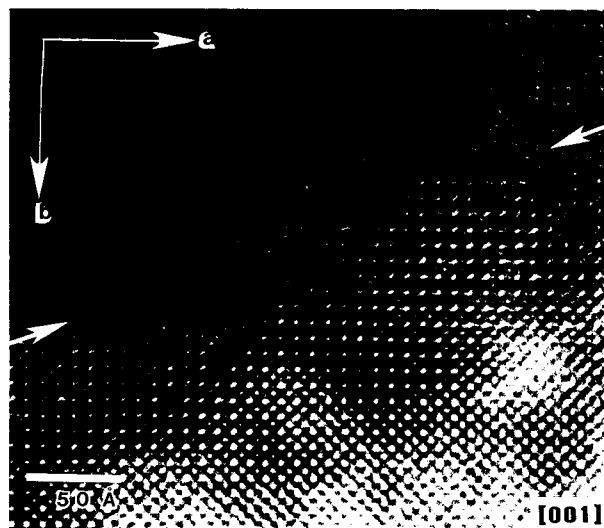


Fig. 14. [001] image of nosean showing an APB (arrows) across which the fringes are shifted by  $\frac{1}{2}a_0$  (best seen by sighting along *b*).

### CONCLUSIONS

The SAED patterns of nosean indicate that the structure is modulated in several directions and that the modulations are incommensurate; the modulations are more prominent along directions such as  $\langle 001 \rangle$ ,  $\langle 110 \rangle$ ,  $\langle 112 \rangle$ ,  $\langle 41\bar{2} \rangle$ , and  $\langle 3\bar{3}1 \rangle$ . The absence of satellite reflections along  $\langle 111 \rangle^*$  directions indicates that ordering does not occur along  $\langle 111 \rangle$ .

HRTEM [001] images provide evidence for ordering of  $[\text{Na}_4 \cdot \text{SO}_4]^{2+}$  and  $[\text{Na}_4 \cdot \text{H}_2\text{O}]^{4+}$  clusters in nosean. The ordering of these clusters having different sizes and charges accounts for the two well-resolved framework oxygen-atom positions. Type 2 domains arise from the ordering of such clusters, and these domains are separated by APBs; the space group for such domains is *P*23. Partial cluster ordering accounts for the positional modulations of the framework oxygen atoms over the O1 and O2 positions and gives rise to the complex satellite reflections. Sodalite- and cancrinite-group minerals provide experimental SAED patterns characteristic of displacive and density modulations, respectively, and they confirm the calculations suggesting that SAED patterns can be used to distinguish displacive vs. density modulations.

### ACKNOWLEDGMENTS

We thank John Barry for useful suggestions and for his help in using and taking some of the pictures on the 4000EX microscope. We also thank the two anonymous reviewers and the Associate Editor, R. J. Reeder, for useful comments on this manuscript. The nosean samples were provided by Fred J. Wicks of the Royal Ontario Museum. This work is supported by NSF grants EAR-8408169 and EAR-8708169; microscopy was done at the ASU HREM facility, which is supported by NSF and ASU.

### REFERENCES CITED

Beagley, B., Henderson, C.M.B., and Taylor, D. (1982) The crystal structures of aluminosilicate-sodalites: X-ray diffraction studies and computer modelling. *Mineralogical Magazine*, 46, 459–464.

- Belokoneva, E.L., Dem'yanets, L.N., Uvarova, T.G., and Belov, N.V. (1982) Crystal structure of Ge sodalite  $\text{Na}_6\text{Al}_6\text{Ge}_6\text{O}_{24}(\text{OH})_2$ . *Soviet Physics. Crystallography*, 27, 597–598.
- Buseck, P.R., and Cowley, J.M. (1983) Modulated and intergrowth structures in minerals and electron microscope methods for their study. *American Mineralogist*, 68, 18–40.
- Cowley, J.M., and Moodie, A.F. (1957) The scattering of electrons by atoms and crystals: I. A new theoretical approach. *Acta Crystallographica*, 10, 609–619.
- Dano, M. (1966) The crystal structure of tugtupite—A new mineral,  $\text{Na}_6\text{Al}_2\text{Be}_2\text{Si}_8\text{O}_{24}(\text{Cl},\text{S})_2$ . *Acta Crystallographica*, 20, 812–816.
- Depmeier, W. (1984) Aluminate sodalite  $\text{Ca}_8[\text{Al}_{12}\text{O}_{24}](\text{WO}_4)_2$  at room temperature. *Acta Crystallographica*, C40, 226–231.
- Goodman, P., and Moodie, A.F. (1974) Numerical evaluation of N-beam wave functions in electron scattering by the multi-slice method. *Acta Crystallographica*, A30, 280–290.
- Grundy, H.D., and Hassan, I. (1982) The crystal structure of a carbonate-rich cancrinite. *Canadian Mineralogist*, 20, 239–251.
- Hassan, I. (1983) The crystal chemistry and crystal structure of the sodalite and cancrinite groups of minerals. Ph.D. thesis, McMaster University, Hamilton, Ontario, Canada.
- Hassan, I., and Buseck, P.R. (1987) The incommensurate-modulated structures of sodalite-group minerals. *Geological Society of America Abstracts with Programs*, 19, 695.
- (1988) A HRTEM characterization of scapolite solid-solutions. *American Mineralogist*, 73, 119–134.
- (1989) Cluster ordering and antiphase domain boundaries in hauyne. *Canadian Mineralogist*, in press.
- Hassan, I., and Grundy, H.D. (1983a) Structure of basic sodalite,  $\text{Na}_6\text{Al}_6\text{Si}_6\text{O}_{24}(\text{OH})_2 \cdot 2\text{H}_2\text{O}$ . *Acta Crystallographica*, C39, 3–5.
- (1983b) The crystal structure of nosean. *Geological Association of Canada Abstracts with Programs*, 8, A30.
- (1984a) The crystal structures of sodalite-group minerals. *Acta Crystallographica*, B40, 6–13.
- (1984b) The character of the cancrinite-vishnevitte solid-solution series. *Canadian Mineralogist*, 22, 333–340.
- (1985) The crystal structures of helvite group minerals,  $(\text{Mn},\text{Fe},\text{Zn})_6(\text{Be}_6\text{Si}_6\text{O}_{24})\text{S}_2$ . *American Mineralogist*, 70, 186–192.
- (1989a) The structure of nosean, ideally  $\text{Na}_6[\text{Al}_6\text{Si}_6\text{O}_{24}]\text{SO}_4 \cdot \text{H}_2\text{O}$ . *Canadian Mineralogist*, in press.
- (1989b) The structure of davyne and its implications regarding stacking faults. *Canadian Mineralogist*, in press.
- Hassan, I., Peterson, R.C., and Grundy, H.D. (1985) The structure of lazurite, ideally  $\text{Na}_6\text{Ca}_2(\text{Al}_6\text{Si}_6\text{O}_{24})\text{S}_2$ , a member of the sodalite group. *Acta Crystallographica*, C41, 827–832.
- Hirsh, P., Howie, A., Nicholson, R.B., Pashley, D.W., and Whelan, M.J. (1977) *Electron microscopy of thin crystals*. Krieger, Huntington, New York.
- Ito, T., and Sadanaga, R. (1966) On the polysynthetic structure of hauyne (abs.). *Acta Crystallographica*, 21, A55.
- Lohn, J., and Schulz, H. (1968) Strukturverfeinerung am gestorten hauyn,  $(\text{Na}_3\text{K},\text{Ca}_2)\text{Al}_6\text{Si}_6\text{O}_{24}(\text{SO}_4)_{1.5}$ . *Neues Jahrbuch für Mineralogie Abhandlungen*, 109, 201–210.
- McCusker, L.B., Meier, W.M., Suzuki, K., and Shin, S. (1986) The crystal structure of a sodium gалlosilicate sodalite. *Zeolites*, 6, 388–391.
- Morimoto, N. (1978) Incommensurate superstructures in transformation of minerals. *Recent Progress of Natural Sciences in Japan*, vol. 3, 183–206.
- O'Keefe, M.A., and Buseck, P.R. (1979) Computation of high resolution TEM images of minerals. *Transactions of the American Crystallographic Association*, 15, 27–44.
- O'Keefe, M.A., Buseck, P.R., and Iijima, S. (1978) Computed crystal structure images for high resolution electron microscopy. *Nature*, 274, 322–324.
- Peterson, R.C. (1983) The crystal structure of hackmanite, a variety of sodalite, from Mont St-Hilaire, Quebec. *Canadian Mineralogist*, 21, 549–552.
- Ponomarev, V.I., Kheiker, D.M., and Belov, N.V. (1971) Crystal structure of tetracalcium trialuminate—The aluminate analog of sodalite. *Soviet Physics. Crystallography*, 15, 799–801.

- Saalfeld, H. (1959) Untersuchung über die nosean-Struktur. *Neues Jahrbuch für Mineralogie Monatshefte*, 38–46.
- (1961) Strukturbesonderheiten des hauyngitters. *Zeitschrift für Kristallographie*, 115, 132–140.
- Sahl, K. (1980) Refinement of the crystal structure of bicchulite,  $\text{Ca}_2(\text{Al}_2\text{SiO}_6)(\text{OH})_2$ . *Zeitschrift für Kristallographie*, 152, 13–21.
- Schulz, H. (1970) Struktur- und Überstrukturuntersuchungen an nosean-einkristallen. *Zeitschrift für Kristallographie*, 131, 114–138.
- Schulz, H., and Saalfeld, H. (1965) Zur Kristallstruktur des noseans,  $\text{Na}_8[\text{SO}_4(\text{Al}_6\text{Si}_6\text{O}_{24})]$ . *Tschermaks Mineralogische und Petrographische Mitteilungen*, 10, 225–232.
- Smith, J.V. (1974) *Feldspar minerals*. Vol. 1—Crystal structure and physical properties. Springer-Verlag, New York.
- Smith-Verdier, P., and Garcia-Blanco, S. (1980) Redetermination of the structure of anhydrous zinc metaborate  $\text{Zn}_4\text{O}(\text{BO}_2)_6$ . *Zeitschrift für Kristallographie*, 151, 175–177.
- Taylor, D. (1967) The sodalite group of minerals. *Contribution to Mineralogy and Petrology*, 16, 172–188.
- Tsuchiya, N., and Takéuchi, Y. (1985) Fine texture of hauyne having a modulated structure. *Zeitschrift für Kristallographie*, 173, 273–281.
- Williams, D.B. (1984) *Practical analytical electron microscopy in materials science*, p. 129–132. Philips Electronic Instruments, Inc., Mahwah, New Jersey.

MANUSCRIPT RECEIVED FEBRUARY 4, 1988

MANUSCRIPT ACCEPTED OCTOBER 5, 1988